JGR Oceans

RESEARCH ARTICLE
10.1029/2022JC019361

Mesoscale Circulation Controls Chlorophyll Concentrations in the East Australian Current Separation Zone

Neil Malan[1,2], **Moninya Roughan**[1,2], **Michael Hemming**[1,2], **and Amandine Schaeffer**[2,3]

[1]Coastal and Regional Oceanography Lab, School of Biological Earth and Environmental Sciences, UNSW Sydney, Sydney, NSW, Australia, [2]Centre for Marine Science and Innovation, UNSW Sydney, Sydney, NSW, Australia, [3]School of Mathematics and Statistics, UNSW Sydney, Sydney, NSW, Australia

Key Points:

- Mesoscale circulation has a strong influence on shelf stratification and chlorophyll distribution with implications for oceanic CO_2 uptake
- EAC separation modulates the upwelling processes which drive a stronger chlorophyll response during summer at depth
- A re-occurring EAC eddy dipole results in an enhanced subsurface chlorophyll maximum and increased cross-shelf exchange

Supporting Information:

Supporting Information may be found in the online version of this article.

Correspondence to:

N. Malan,
n.malan@unsw.edu.au

Citation:

Malan, N., Roughan, M., Hemming, M., & Schaeffer, A. (2023). Mesoscale circulation controls chlorophyll concentrations in the East Australian current separation zone. *Journal of Geophysical Research: Oceans*, *128*, e2022JC019361. https://doi.org/10.1029/2022JC019361

Received 5 OCT 2022
Accepted 14 MAR 2023

Author Contributions:

Conceptualization: Neil Malan, Moninya Roughan, Amandine Schaeffer
Data curation: Neil Malan
Formal analysis: Neil Malan, Michael Hemming
Funding acquisition: Moninya Roughan
Investigation: Neil Malan, Moninya Roughan, Amandine Schaeffer
Methodology: Neil Malan, Michael Hemming, Amandine Schaeffer
Project Administration: Moninya Roughan
Visualization: Neil Malan
Writing – original draft: Neil Malan

Abstract Understanding the distribution of chlorophyll on the continental shelves adjacent to western boundary currents is important, both from an ecosystem perspective, as well as for their role as a net sink of atmospheric CO_2. However, in-situ observations of chlorophyll in these dynamic regions are rare. Here, using more than a decade of underwater glider observations from 29 deployments in the East Australian Current (EAC) system, we examine the effect of the mesoscale western boundary current (WBC) circulation on chlorophyll distribution across the shelf. The extensive hydrographic dataset reveals that the mode of boundary current separation has a strong persistent spatial influence on both the stratification and chlorophyll distribution on the shelf between 31.5° and 34°S, a productive area adjacent to the EAC separation zone. We identify that subsurface chlorophyll maxima are common, and their depth and strength is dictated by the offshore mesoscale circulation associated with the WBC separation. The vertical chlorophyll distribution is modulated by the combination of the seasonal cycle and the sporadic influence of mesoscale eddies associated with WBC jet separation. Of the three dominant WBC separation scenarios, eddy dipoles result in shelf waters that are on average more stratified, have higher chlorophyll values, and a deeper chlorophyll maximum compared to other circulation modes. These results suggest that it is necessary to consider the influence of WBC dynamics on chlorophyll concentrations for accurate estimates of atmospheric CO_2 uptake.

Plain Language Summary In the past, our understanding of chlorophyll distributions in East Australian Current came mainly from satellite data. However, satellites cannot see far below the surface of the ocean. We use data from a decade of underwater glider missions to look at subsurface chlorophyll and find that the East Australian Current and its eddies strongly influence shelf chlorophyll at depth, even giving it a different seasonal cycle to the surface. We think that this is important for how this region takes up carbon dioxide from the atmosphere.

1. Introduction

Continental shelf waters account for a disproportionate share of oceanic primary production, supporting many of the world's largest fisheries (Pauly & Christensen, 1995) despite only accounting for 8% of the total ocean surface area, and an even smaller percentage of ocean volume. However, our estimates of primary production at a global scale are poorly constrained (Carr et al., 2006) and rely on satellite-derived chlorophyll which can perform poorly close to the coast (Jacox et al., 2015), can be inhibited by cloud cover and do not fully capture subsurface dynamics (Oliver et al., 2021).

Traditionally, eastern boundary current systems such as the California Current and Benguela upwelling system have been the focus of much research into biological productivity, due to the large amount of biomass and therefore fisheries that they support (Carr & Kearns, 2003; Pauly & Christensen, 1995; Renault et al., 2016). Western boundary current systems on the other hand, while still important in supporting local fisheries, are less productive in absolute terms. However, western boundary current systems play an important role in the climate system as a sink of atmospheric carbon dioxide, with a combination of strong air-sea heat-fluxes and the biological production making western boundary currents hotspots of ocean carbon uptake (Fassbender et al., 2018; Nickford et al., 2022).

As western boundary currents have energetic dynamics, strong velocities that drive cross-shore gradients, and high levels of variability, studies of chlorophyll dynamics on their adjacent shelves are somewhat rare and generally rely on satellite-derived chlorophyll concentrations (e.g., Everett et al., 2014; Schollaert et al., 2004).

Writing – review & editing: Neil Malan, Moninya Roughan, Michael Hemming, Amandine Schaeffer

However, these same energetic eddies and fronts, which make understanding steady-state chlorophyll dynamics on western boundary current shelves challenging, have also been shown to be important for the uptake of particulate organic carbon via subduction mechanisms (Levy et al., 2013; Omand et al., 2015). Thus, in addition to its role in supporting local fisheries, understanding chlorophyll dynamics in energetic regions such as western boundary currents and their continental shelves is important in the context of global climate.

Along the east coast of Australia, Everett et al. (2014), using satellite data, found a maximum in shelf chlorophyll concentrations between 31.5°S and 34°S associated with the separation of the East Australian Current (EAC) along a wider region of the continental shelf of eastern Australia known as the Hawkesbury Shelf. The Hawkesbury Shelf at times contains more than 20% of the total chlorophyll on the shelf of the east coast of Australia despite accounting for less than 10% of the total shelf length (Everett et al., 2014). It was found that shelf chlorophyll concentrations were controlled by both wind- and current-driven upwelling processes. This finding was in agreement with earlier work (Oke & Middleton, 2001) that had hypothesized that phytoplankton blooms in the Hawkesbury Shelf region were caused by downstream advection of nutrients upwelled by interaction with topography. Roughan and Middleton (2002) however, in their examination of upwelling mechanisms in the region, found that upwelling driven by the separation of the EAC jet from the coast was responsible for maintaining the nutrient pool on the shelf. The role of separation-driven upwelling in maintaining persistent bottom water uplift on the Hawkesbury Shelf was later confirmed using repeat glider measurements (Schaeffer & Roughan, 2015). Eddy encroachment onto the shelf has also been identified as an important process driving cross-shelf transport (Malan et al., 2022; Roughan et al., 2022) and productivity, in agreement with studies using in-situ shipboard observations (Mullaney & Suthers, 2013; Roughan et al., 2017) and numerical models (Cetina-Heredia, Roughan, Liggins, et al., 2019).

The Hawkesbury Shelf is located where the Australian coastline bends west, adjacent to where the coherent, poleward-flowing jet of the EAC usually separates from the coast between 30.7°S and 32.4°S (Cetina-Heredia et al., 2014). The dynamics of this separation is controlled by the shedding of large mesoscale anticyclonic eddies which dominate the southern extension of the EAC. The southward penetration of the EAC jet is at its greatest immediately before an anticyclonic eddy is shed, whereupon the jet then retracts back equatorward (Cetina-Heredia et al., 2014).

Recent work has revealed an additional complexity to this highly dynamic separation process; cyclonic eddies have been observed to propagate westward (Cetina-Heredia, Roughan, Sebille, et al., 2019), impacting the separation of the jet (Li et al., 2022b) and are often found in the region alongside anticyclonic eddies, forming eddy dipoles (Cetina-Heredia, Roughan, Liggins, et al., 2019). These eddy dipoles are present in some configuration more than 50% of the time (Malan et al., 2020) and can direct a strong jet of offshore water directly onshore (Archer et al., 2020; Cetina-Heredia, Roughan, Liggins, et al., 2019) toward the productive Hawkesbury Shelf. On the shelf, inshore of the 200 m isobath, the dynamics are different, although mesoscale circulation still plays a role (Li et al., 2022; Ribbat et al., 2020; Roughan et al., 2022). Due to their depth, large mesoscale eddies are restricted from directly impinging onto and across the shelf edge (Pilo et al., 2018), confirmed by drifter observations showing that the surface flow of a shoreward eddy dipole jet does not cross the 1,000 m isobath (Malan et al., 2020).

Ribbat et al. (2020) applied an empirical orthogonal function analysis to both a 2 years high resolution (750 m) ocean model, as well as geostrophic velocities derived from altimetry (approx 25 km resolution) in order to understand the different modes of variability of waters in the EAC separation region. They identify the first empirical orthogonal function mode as the "EAC mode" where the system is dominated by the poleward flowing EAC, representing 47.3% of the variance over the satellite altimetry record and 53.8% of the variance over the 2-year model run period. The second is the "EAC eddy mode" where the EAC separates in the north of our domain, and a cyclonic eddy is present at the shelf break (representing 20.1% and 12.4% of the variance in satellite altimetry and model, respectively). The third mode is the "Eddy dipole mode" where an anticyclone/cyclone eddy dipole lies downstream of the EAC separation (representing 13.4% and 10.5% of the variance in AVISO and model, respectively). These modes were further refined by Roughan et al. (2022) who showed that they control the transport of water across the shelf. These modes provide a useful framework for understanding the variability in the EAC separation zone. We will refer to them as follows; (a) "EAC" mode where the shelf edge is dominated by a coherent, poleward flowing current, (b) "Eddy" mode, where the EAC separates further to the north and a single cyclonic eddy is present adjacent to the shelf, and (c) "Dipole" mode, where two counter-rotating eddies

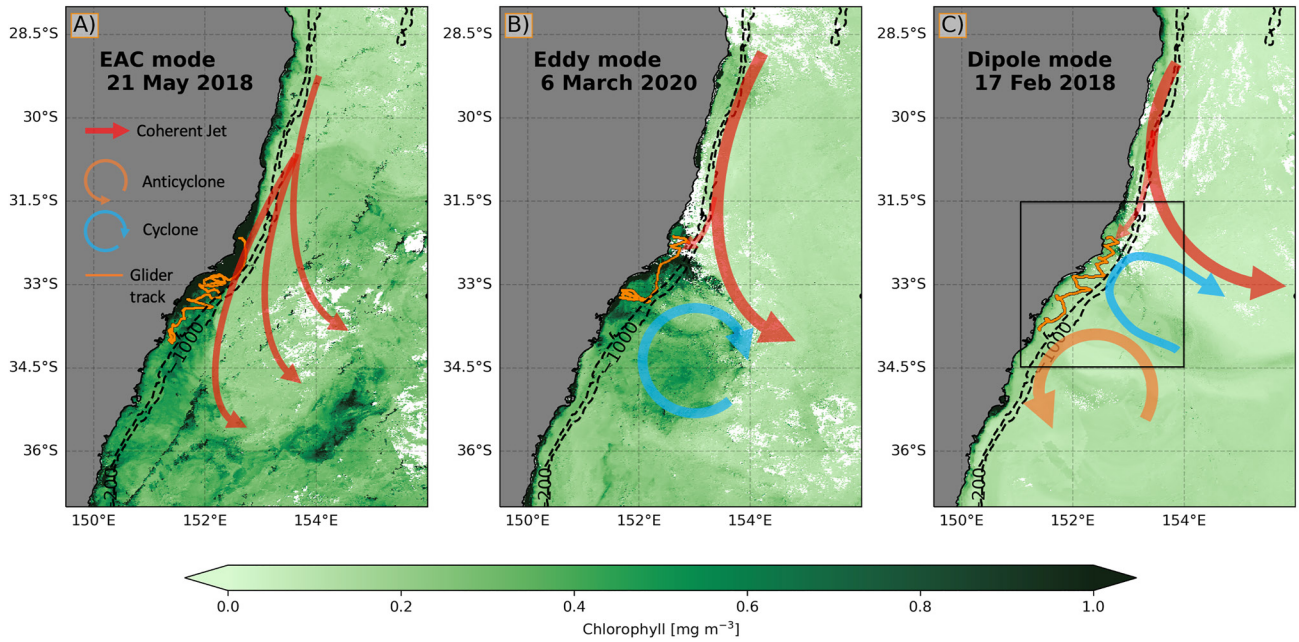

Figure 1. 8-day composites of MODIS chlorophyll concentrations, centered on the case study dates of (a) EAC mode, (b) Eddy mode, and (c) Dipole mode. The tracks of the glider missions used for the case studies are marked in orange. Overlaid is a schematic of the currents and associated modes of EAC separation, adapted from Ribbat et al. (2020) and Roughan et al. (2022). The 200 and 1,000 m isobaths are shown by black dashed contours. The domain covered by Figure 4 is shown by the black box on panel (c).

are present downstream of the EAC jet, forming an eddy dipole structure and driving onshore cross-shelf flow which impacts the shelf. These modes are shown schematically in Figure 1.

2. Approach

Knowledge of the mesoscale variability and dynamics of the EAC system is growing, including separation dynamics, eddy-shedding (Bull et al., 2017; Cetina-Heredia et al., 2014; Li et al., 2021), and trends (Li et al., 2022a, 2022b; Malan et al., 2021). However, the extent to which this mesoscale variability controls the shelf circulation at smaller, biologically relevant scales, and thus the productivity of the Hawkesbury Shelf, is less clear. Most previous studies of productivity in the EAC system make use of surface satellite-derived chlorophyll measurements, shorter process studies and some opportunistic sampling. With subsurface chlorophyll maxima being ubiquitous in much of the global ocean (Cullen, 2015), and previously observed by underwater gliders on the EAC shelf (Schaeffer, Roughan, Jones, & White, 2016), it is almost certain that much of the variability in chlorophyll distribution on the Hawkesbury Shelf has gone undetected.

To explore the subsurface chlorophyll distribution, in this paper we use hydrographic data from 29 ocean glider missions (Section 3) carried out over a period of more than a decade. We combine these data with satellite data and 3 years of high-resolution surface currents from an HF radar system (Section 4.1.1), to examine how mesoscale variability in the EAC circulation in the separation zone controls the 3-dimensional chlorophyll concentration and distribution in the Hawkesbury Shelf region (Sections 4.1.2 and 4.2). We discuss the results in the context of EAC separation modes and their possible impact on subsurface chlorophyll and CO_2 uptake in Section 5.

3. Materials and Methods

3.1. Satellite Remote Sensing

Several satellite remote sensing products are used to assess the mesoscale circulation, as well as the surface conditions on the continental shelf. Gridded sea level anomaly and surface geostrophic velocities are obtained from an OceanCurrent product distributed by Australia's Integrated Marine Observing System (IMOS) that merges satellite altimetry with sea level elevation measurements from coastal tide gauges (Deng et al., 2011) to

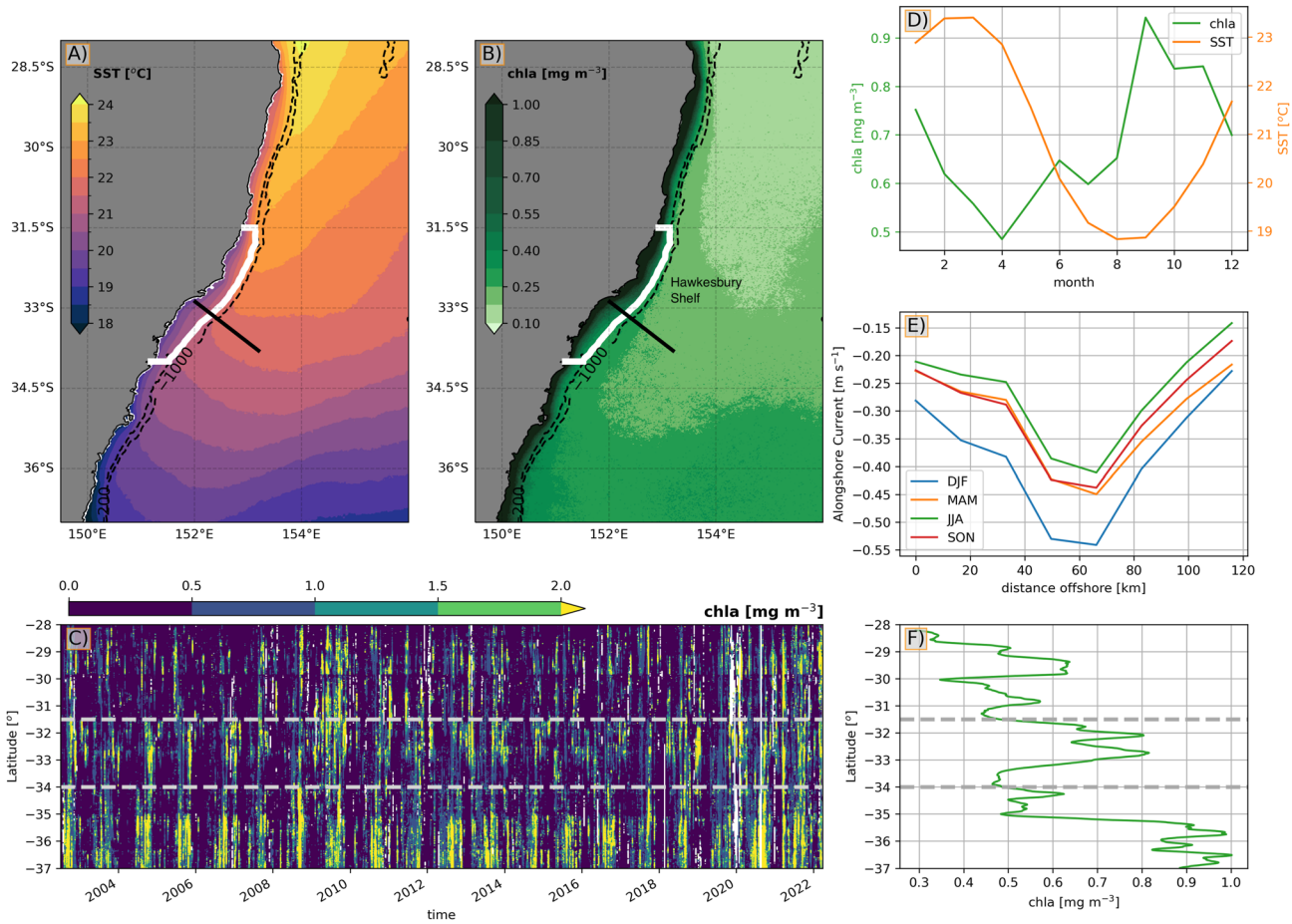

Figure 2. (a) Time-mean satellite sea surface temperature, black dashed contours show the 200 and 1,000 m isobaths, the white box shows the Hawkesbury Shelf area of interest used for calculating the seasonal cycle, and the black transect shows the section used to quantify the along-shore geostrophic current. (b) As for previous panel, but showing time-mean satellite-derived chlorophyll concentrations. (c) Latitude-time plot of shelf chlorophyll (averaged from coast to 200 m isobath). (d) The seasonal cycle of satellite sea surface temperature and chlorophyll, area-averaged over the white box. (e) Along-shore geostrophic velocities, rotated normal to the black section in panel (a) and averaged seasonally. (f) Time-mean of shelf chlorophyll with latitude, gray dashed lines show the latitudinal extent of the Hawkesbury Shelf area of interest.

improve accuracy in coastal regions. This product has been shown to resolve the mesoscale EAC system well in several previous studies (Deng et al., 2011; Malan et al., 2020; Pilo et al., 2018). Spatial resolution is 0.2° and the temporal coverage is from 1993 to present. Daily satellite sea surface temperature (SST) is obtained from the IMOS day and night-time L3S product derived from the AVHRR instruments on NOAA polar orbiting satellites (Griffin et al., 2017). The SST data have a spatial resolution of 0.02° and a temporal range from 1992 to present. Daily chlorophyll-a estimates derived from ocean color are obtained from the IMOS MODIS 1 day product, using the OC3 algorithm (Schroeder et al., 2017) at a resolution of 4 km. Note that we refer to both chlorophyll-a concentration estimates from MODIS satellite ocean color using the OC3 algorithm and in situ estimates of chlorophyll-a concentration derived from chlorophyll-a fluorescence from the WET Labs puck mounted on a Slocum glider as chlorophyll (chla). From here on, when necessary, we will denote satellite-derived variables as "$_{sat}$" (i.e., satellite-derived chlorophyll-a will be denoted as chla$_{sat}$).

3.2. Study Region

The study region (31.5°S–34°S, surrounded by a thick white line in Figure 2a) encompasses the Hawkesbury Shelf and is an area of wider shelf inshore of the EAC. It lies astride the approximate location where the EAC transitions from a coherent, poleward-flowing jet to a more variable flow consisting mainly of large mesoscale eddies, which vary in their configuration, causing the three main separation modes described above. This transition can be seen in the time-mean SST isotherms (Figure 2a), which lay approximately along-shore in the

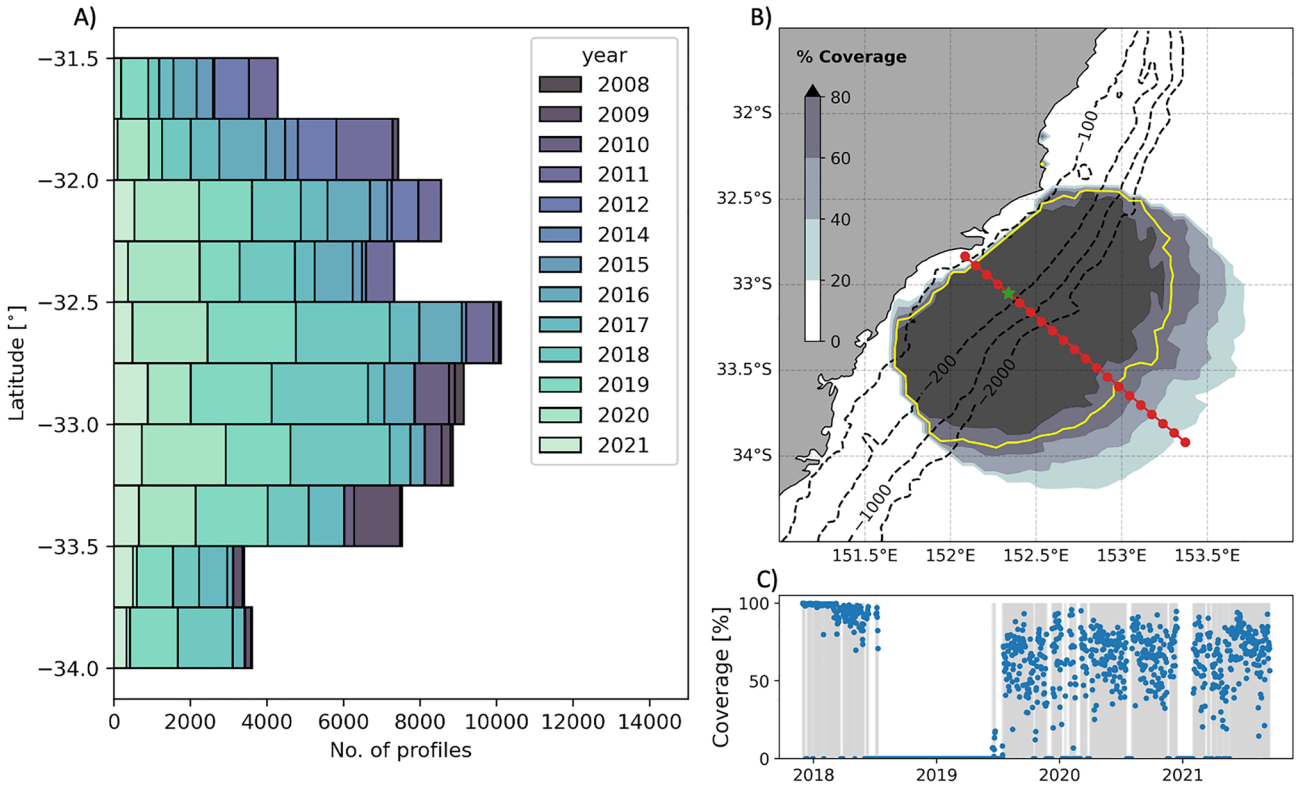

Figure 3. (a) Distribution by latitude of glider profiles used in this study, color indicates the year the profiles were taken. (b) Map of percent data coverage over time for each radar grid cell (the 12 months 2018–2019 of radar shutdown is excluded). The contour of 70% spatial data coverage is shown in yellow. The 100, 200, 1,000, and 2,000 m depth contours are shown as black dashed contours. The transect used for examining along-shelf geostrophic flow patterns (Figure 2e) is shown in red. (c) Blue dots show a time series of radar coverage normalized by the maximum spatial footprint coverage. Gray shading shows the times when the radar was operational, with the large white gap showing the 12 months shutdown for regulatory reasons.

coherent jet region (equatorward of 31.5°S and change to a cross-shore alignment poleward of 34°S. A similar pattern can be seen in the time-mean $chla_{sat}$ (Figure 2b), with low values equatorward of 31.5°S and increasing with latitude. Close along the coast, $chla_{sat}$ values are high, in the so-called "green ribbon" (Lucas et al., 2011; Roughan et al., 2022). When explored over the last 20 years (Figures 2c and 2f), $chla_{sat}$ generally increases with latitude, with lower values in the subtropics of the upstream EAC region than in the more temperate waters poleward of 35°S. However, between 31.5°S and 34°S, there is a peak in the mean shelf $chla_{sat}$ (Figure 2f), previously identified by Everett et al. (2014) and associated with the Hawkesbury Shelf region.

The seasonal cycle of satellite SST and $chla_{sat}$ (spatially averaged from 31.5°S to 34°S inshore of the 200 m isobath) shows temperature peaking in February/March and reaching a minimum in August (Figure 2d). $Chla_{sat}$ shows a typical spring bloom in September and a minimum in April. Along-shelf geostrophic currents (Figure 2e, across the transect (black line) shown in Figure 2a) are strongest December to February with mean values of up to 0.54 m s^{-1}, reducing to <0.45 m s^{-1} in other seasons. The maximum in $chla_{sat}$ over the Hawkesbury Shelf region is clear when taking the time-mean of shelf $chla_{sat}$ (Figure 2f), with the gray dashed lines in Figure 2f showing the area of interest for this study.

3.3. Ocean Gliders

Regular ocean glider missions have been carried out along the inshore edge of the EAC (29.5–35°S) between 2008 and 2021 (Figure 3a) as part of IMOS (Roughan et al., 2015). Earlier versions of this dataset have been used to understand shelf temperature variability and momentum balances (Schaeffer et al., 2014; Schaeffer & Roughan, 2015) as well as physical and biogeochemical scales of variability (Schaeffer, Roughan, Jones, & White, 2016). Due to the inherent difficulties of piloting gliders that are slower than the speed of the EAC itself, the gliders are deployed upstream at either Yamba (29.5°S) or Forster (32.1°S) and retrieved downstream between 33°S and 34°S. To avoid being advected offshore by the EAC, the gliders sample poleward in a zigzag pattern,

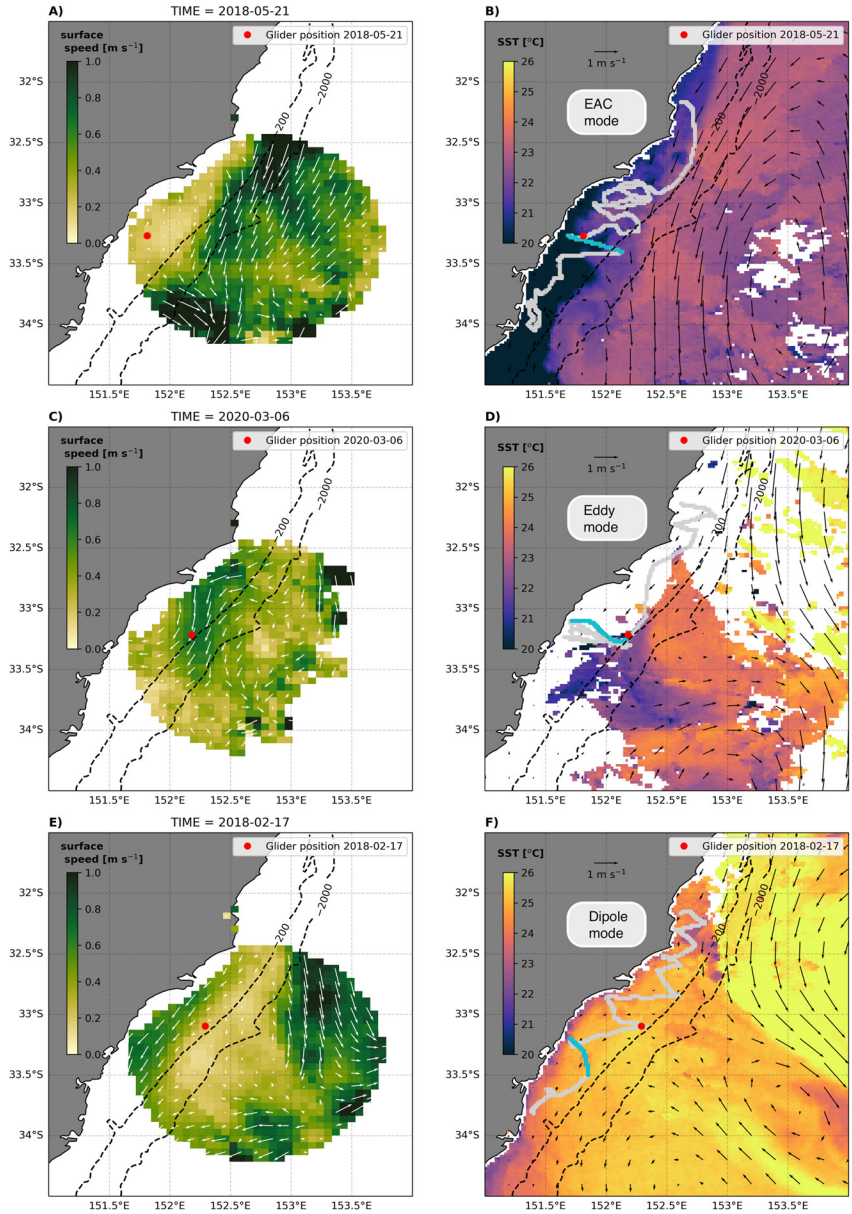

Figure 4. Snapshots exemplifying the three modes of EAC separation, on days where there is a glider under the HF radar footprint, EAC mode (21 May 2018, panels (a)–(b), eddy mode (6 March 2020), panels (c)–(d) and dipole mode (17 of February 2018). In the left-hand panels (a), (c), (e) the vectors are surface ocean current direction, and the shading is surface ocean current magnitude, both from HF radar. In the right-hand panels (b), (d), (f) the vectors show satellite derived geostrophic velocity, and the shading is sea surface temperature. Gray track shows path of concurrent glider mission, the blue track shows the glider data subset used to plot sections in Figure 5.

rather than the more conventional endurance lines undertaken in other more dynamically quiescent regions (Roughan et al., 2015; Testor et al., 2019; Todd et al., 2019). All IMOS gliders are equipped with Seabird-CTD sensor, measuring temperature, salinity and depth, as well as a WET Labs ECO Puck measuring optical properties (chlorophyll-a fluorescence, as well as colored dissolved organic matter and backscatter, not used in this study). The shallow water Slocum gliders sample between the coast and the 200 m isobath from the surface to bottom, with 4–5 missions being undertaken each year. Each mission lasts three to 4 weeks depending on operational constraints such as battery life and weather conditions. This deployment strategy allows quasi-synoptic sampling of the shelf waters inshore of the EAC, with gliders deployed throughout the year (Roughan et al. (2015); Schaeffer and Roughan (2015); Schaeffer, Roughan, Austin, et al. (2016); Schaeffer, Roughan, Jones, and White (2016)).

In this paper, extending the approach used by Schaeffer and Roughan (2015) to include biological variables, we consider vertical hydrographic profiles taken by gliders between the latitudes of 31.5°S and 34°S, and between the coast and the 200 m isobath. We use 29 glider missions undertaken in the area of interest, with data having undergone standard IMOS QA/QC procedures (Woo, 2019). Each mission provides between 3,000 and 6,000 quasi-synoptic hydrographic profiles which are divided into individual profiles, with the average distance between profiles being approximately 200 m. The spatio-temporal coverage of the profiles are shown in Figure 3a. The profiles are vertically gridded onto a 1 m grid, and temperature, salinity, and chlorophyll-a fluorescence are despiked using the median filter and standard deviation bounds methods from GliderTools (Gregor et al., 2019). From here on, where necessary we will denote glider variables with the subscript *glider*. For this study, density is shown as potential density anomaly with a reference pressure of 0 dbar ($\sigma 0$). It must be noted that as systematic bottle samples for calibration of chlorophyll-a fluorescence are not available, there is the possibility of instrument-to-instrument variability between fluorometers. Using data from 26 of our glider missions (i.e., much of the same dataset as this study), Schaeffer, Roughan, Austin, et al. (2016), performed a thorough investigation of offsets between sensors using dark counts (taken as offshore deep measurements for each glider mission), and found offsets of less than 0.1 mg m^{-3} Schaeffer, Roughan, Austin, et al. (2016) also compared surface glider chlorophyll values with satellite data, and despite the effects of submesoscale variability, found a correlation coefficient of $r^2 = 0.69$. Hence the effect of instrument-to-instrument variability is likely small. Further, we assume that any bias would be randomly spread across the three modes of EAC separation used to create the composite means used in our analysis. As our analysis focuses on the difference in subsurface chlorophyll structure, rather than absolute values, we are confident that the possibility of small differences between sensors will not impact our results. Two fluorometers in fact account for 13 of the glider missions used in this study, and do not appear to show any systematic bias over time, or when compared to each other. The seasonal cycle of $chla_{sat}$ and SST on the Hawkesbury Shelf (Figure 2d) is used to split the glider dataset into "warm months" (November–April, where sea surface temperature is high and $chla_{sat}$ is low) and "cool months" (May–October, where the converse is true) later in the analysis.

3.4. High Frequency Coastal Radar

Since 2017, surface currents on the Hawkesbury Shelf have been monitored by a high frequency (HF) coastal radar system consisting of two SeaSonde crossed loop direction finding stations located at Seal Rocks (32.44°S, 152.54°E) and Red Head (33.01°S, 151.73°E). The system operates at a frequency of 5.3 MHz, with a bandwidth of 14 KHz, providing a maximum range of 200 km and measuring the flow of the top half-meter of the water column at a spatial resolution of 6 km and a temporal resolution of 1 hour. The footprint of the data is collected and processed by the IMOS ocean radar facility; Cosoli and Grcic (2019) provide a detailed breakdown of the processing and quality control procedures. From July 2018 to July 2019, the HF radar system had to be shut down due to frequency and regulatory issues (white gaps in Figure 3c). These issues were resolved by the implementation of "Listen-Before-Talk" mode (Cosoli, 2020) and directional antennae (de Vos et al., 2020) and the system was brought back online in June 2019. The HF radar system provides high-resolution surface current velocities which includes ageostrophic motions, which are not resolved by the satellite-derived geostrophic currents used in previous studies. This is due to the different parameters and resolution measured by the two observing platforms (radar and satellite). The radar directly measures the ocean current velocity in the top layer (~2 m) of the water column, while the satellite-derived velocities use the geostrophic assumption to estimate velocities from the sea surface height, more akin to a depth-integrated flow. The spatial resolution also differs (6 vs. 25 km respectively). Thus, when the surface flow field is complex, or has large vertical shear in velocity, the radar and satellite estimates will differ.The spatial and temporal coverage of the radar system is shown in Figures 3b and 3c.

4. Results

4.1. Case Studies

4.1.1. Surface Circulation

Case studies typical of each of the three EAC separation scenarios identified by Ribbat et al. (2020) (the "EAC mode," "eddy mode" and "dipole mode" configurations) are selected from periods where both HF radar and glider data are available. These three case studies are chosen to be as close to the same period of the year as possible. The EAC mode example is 21 May 2018, the eddy mode example is 6 March 2020 and the dipole mode is 17 February 2018. An examination of 8-day composites of $chla_{sat}$ shows that, as could be expected from our understanding of current-driven upwelling, the EAC mode example shows high $chla_{sat}$ values on the adjacent shelf (~1 mg m^{-3},

Figure 1a), sharply contrasting with the edge of the EAC which is depleted in $chla_{sat}$. The eddy mode (Figure 1b) showed generally lower $chla_{sat}$ values, with less $chla_{sat}$ along the coast on the shelf, and slightly elevated $chla_{sat}$ values (~0.5 mg m^{-3}) offshore associated with the single cyclonic eddy (Figure 1b). The dipole mode (Figure 1c) shows the lowest $chla_{sat}$ values in the entire domain, both on and off the shelf, generally not exceeding 0.3 mg m^{-3}.

We now explore these three examples in greater detail using the glider and HF radar data (Figure 4). In the EAC mode example (21 May 2018), the surface flow field is characterized by a strong (>0.8 m s^{-1}) southwestward current offshore of the 200 m isobath, and low (<0.2 m s^{-1}) velocities on the shelf (Figures 4a and 4b), forming a strong shelf break velocity front. The offshore geostrophic velocities (Figure 4b), show the presence of a typical EAC jet, with ~1 m s^{-1} southwestward velocities.

The eddy mode example (6 March 2020), characterized by the presence of a single mesoscale cyclonic eddy offshore (Figures 4c and 4d) associated with an EAC jet further offshore, appears to show much weaker and variable velocities at the shelf break. There is a bifurcation in the EAC, with flow offshore of the shelf break being directed southeastward, whilst a meandering flow on the shelf travels southwestward (Figure 4c). It should be noted that in both the eddy mode case study (Figures 4c and 4d), and the dipole mode case study (Figures 4e and 4f), there are differences in the flow measured by radar and satellite, meaning that the flow is complex and vertically sheared.

In the dipole mode example (17 February 2018, Figures 4e and 4f), the offshore EAC separation is well represented in the radar surface velocities, and the typical onshore jet resulting from the dipole circulation (highlighted by Malan et al. (2020) and Archer et al. (2020)), is visible (around 34°S). The representation of the cyclonic eddy differs slightly between the HF radar (Figure 4e), where the northeastward flow associated with the cyclonic eddy is only visible right at the edge of the radar footprint (34°S, 153.5°E) and the geostrophic velocities (Figure 4f), where the cyclonic eddy is positioned closer to the shelf edge. The difference is most likely to be caused by the difference in temporal resolution between the underlying data, which is hourly for the HF radar, but interpolated from ~10 days satellite overpasses in the case of the geostrophic velocities. Also notable is the strong (>0.5 m s^{-1}) southwestward flow on the shelf, which is stronger near the coast. The shelf edge velocities are low in contrast to the EAC mode, where they are >1 m s^{-1}.

4.1.2. Vertical Hydrographic Structure

The subsurface structure of the shelf waters associated with the three distinct modes of EAC separation present in the case studies is examined by taking an across-shelf section (~36 hr in duration) of the glider mission during each of the three scenarios (shown in Figure 4). The location of the sections, shown in blue in Figures 4b, 4d, and 4f, are as close to each other geographically as possible (around 33.2°S), while still being close in time to the radar snapshots shown in Figures 4a, 4c, and 4e.

The EAC mode example (Figure 5a) shows the weakest density stratification throughout the shelf. $Chla_{glider}$ (Figure 5b) is mostly distributed in the top 40 m of the water column and, unlike what is seen from the surface in Figure 1a, has the lowest maximum values (1.5 mg m^{-3} at 20 m depth) of the three modes when considering subsurface concentrations. A mean taken across the section for the EAC mode scenario (Figure 5c) reveals a maximum $chla_{glider}$ value of 1.5 ± 0.41 mg m^{-3} at 20 m.

The eddy mode example (Figure 5e) shows strong stratification in the upper 20 m of the water column and corresponding high levels of $chla_{glider}$ inshore, most likely caused by above average rainfall during February 2020 (317 mm of accumulated rainfall recorded during February 2020 at Port Stephens, BoM station 061,054, almost three times higher than the February average of 113 mm, Bureau of Meteorology (2022)). However, the mean of the section (Figure 5f) shows that the effect of this fresh water input is confined to a layer of low density water in the top 15 m of the water column with temperature being the greater contributor to the density structure of the rest of the water column (Figure 6). The $chla_{glider}$ maximum of 1.6 ± 0.73 mg m^{-3} is in the layer of fresher water, at 14 m depth, but otherwise the $chla_{glider}$ profile is similar to that of the EAC mode example above.

The dipole mode example (Figure 5g), shows the strongest density stratification, with a pycnocline at around 40 m, which gradually deepens and strengthens in the offshore direction. $chla_{glider}$ values (Figure 5h), are the strongest (>4 mg m^{-3} at some points) of the three case studies, and show a distinct subsurface maximum, matching the pycnocline as it deepens offshore. The section mean for the dipole mode example (Figure 5i) shows a deep $chla_{glider}$ maximum (2 ± 1.2 mg m^{-3}) at a depth of 40 m.

This pattern of the dipole mode case study having the strongest stratification and highest $chla_{glider}$ concentrations, and the EAC mode case study having the weakest stratification, and lowest $chla_{glider}$ concentrations is also true if

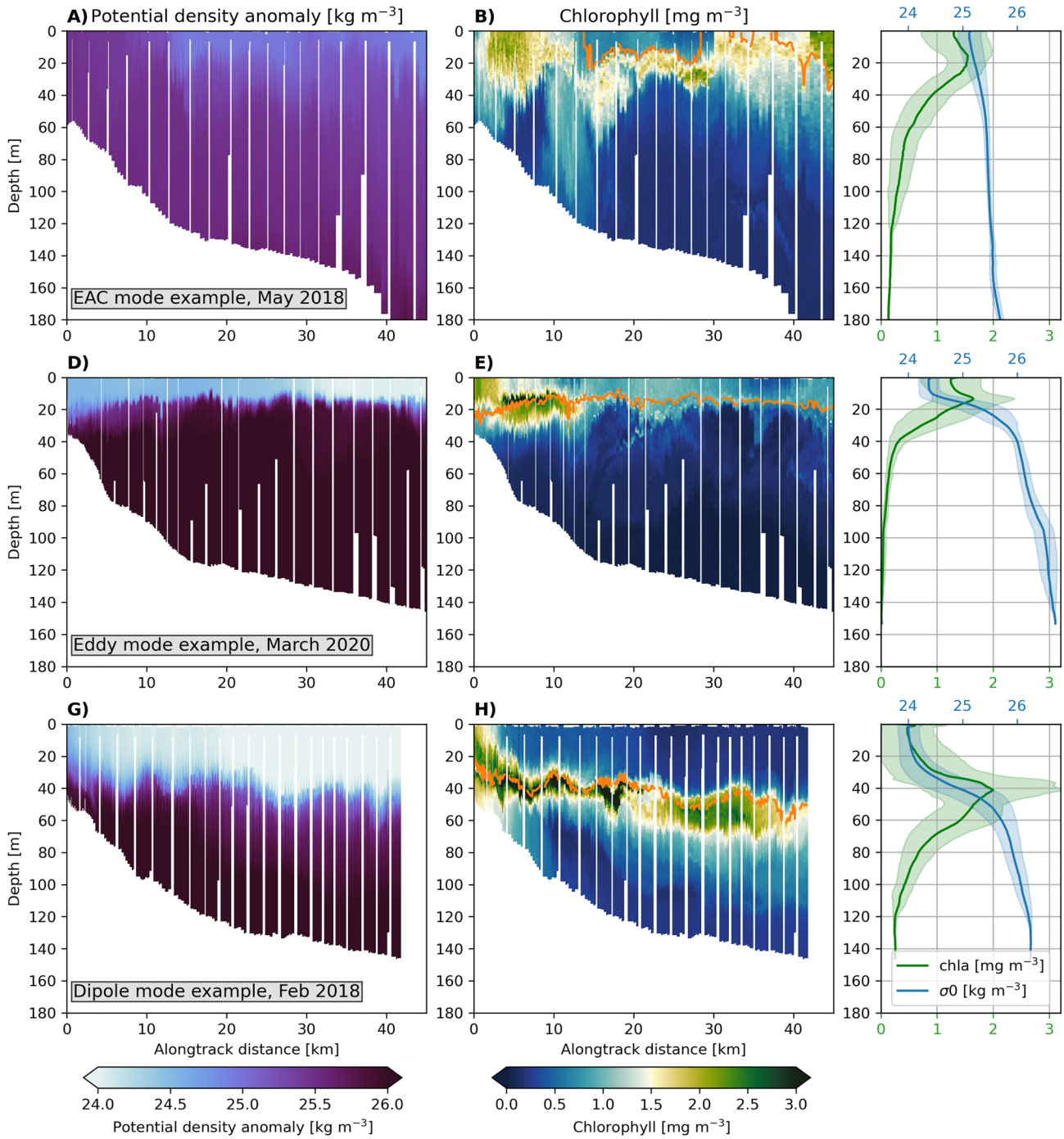

Figure 5. Across-shelf sections (blue glider tracks in Figure 4) of potential density anomaly and chlorophyll concentrations for the EAC mode (a)–(b), EAC eddy mode (d)–(e), and eddy dipole mode (g)–(h), configurations, taken from a subset of the glider missions during the three case studies shown in Figure 4. The orange contour on panels B, E and H shows the position of the 25 kg m^{-3} potential density anomaly contour. Panels C, F, and I show the mean profiles of chlorophyll and potential density anomaly across each section.

you consider the entire glider mission for each case study (shown by the gray tracks in Figures 4b, 4d and 4f). If we consider the time-mean vertical profiles for the duration of each mission (Figure 6), the EAC mode, as was seen in the individual sections, has both the least stratification (Figure 6d), and the lowest maximum $\text{chla}_{\text{glider}}$ values (Figure 6a). The opposite is true for the mission where the EAC separation is in dipole mode. The persistence of these signals in stratification, as well as the depth and magnitude of the subsurface chlorophyll maximum,

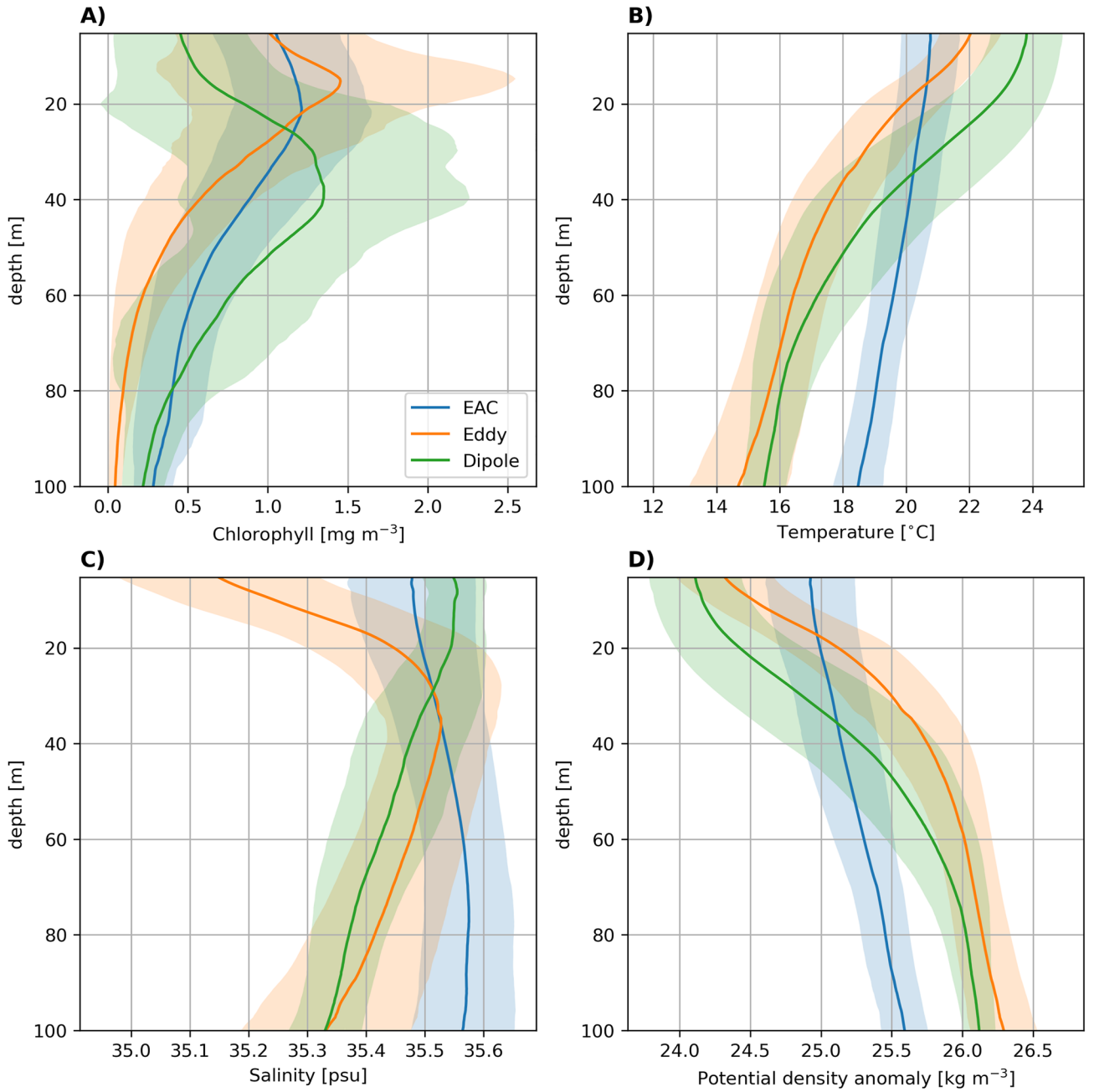

Figure 6. Mean profiles (shaded by standard deviation) of chlorophyll, temperature, salinity and density for the top 100 m of the water column taken over the period where gliders are inshore of the 200 m isobath between 31.5°S and 34°S (gray glider tracks on Figure 4). Colors show the three glider missions chosen for the case studies shown in Figure 4, demonstrating the EAC, eddy and dipole modes of separation.

through the full latitudinal extent of the mission (extending from 32° to 34°S), suggests that the offshore mesoscale has an influence on the vertical distribution of chlorophyll along the length of the Hawkesbury Shelf.

The differences in stratification could be as a result of offshore water being transported onto the shelf and so it is interesting to explore the differences in cross-shelf flows between each mode case study. We consider the satellite geostrophic currents flowing across the 2000 m isobath. The 2000 m isobath is chosen as both satellite altimetry and the geostrophic assumption become less accurate estimations of the total flow the closer one gets to the coast. Geostrophic currents are extracted along the 2000 m isobath, and rotated so as to be normal to its direction, giving an estimate of cross-shelf transport (Figure 7). During the case study of the EAC mode (Figure 7a), the cross-shelf velocities are close to zero between 32°S and 33°S, with large levels of variability between 32.75 and 33.5°S

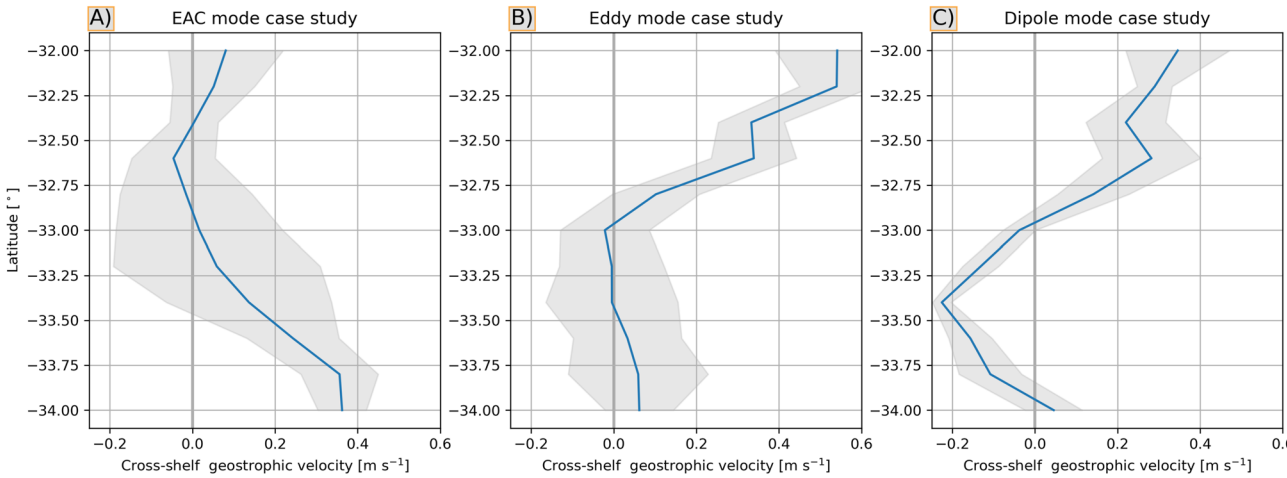

Figure 7. Cross-shelf transport estimated at the 2,000 m isobath from satellite-derived geostrophic velocities, positive values indicate offshore transport. Shading indicates one standard deviation.

relative to other latitudes, where cross-shelf velocities turn consistently offshore and reduce in variability. This is indicative of the coherent EAC jet flowing poleward along the shelf break, before separating from the shelf in the south of the domain, driving the consistent offshore velocities south of 33°S. The eddy mode case study (Figure 7b) shows the footprint of the EAC jet separating further north with strong offshore cross-shelf velocities in the equatorward half of the domain. In a near mirror-image of the EAC mode case, cross-shelf geostrophic velocities return to near-zero poleward of 33°S and increase in their variability. In the dipole mode case study, there is a similar early EAC jet separation, with offshore cross-shelf velocities on the equatorward half of the domain. However, the dipole mode case is unique amongst the three modes in having onshore transport, with a peak in onshore geostrophic velocity at 33.4°S, associated with the contour-rotating eddy dipole driving onshore flow at the shelf break.

4.2. Mean Hydrographic Structure From 29 Glider Missions

The above results come from only three case studies, one for each mode of EAC separation. Does the contrast between the different separation modes hold true considering all days for which we have radar and glider observations of the shelf circulation? To examine whether the effect of EAC separation mode on chlorophyll distribution is robust over time, we assign each of the 29 glider missions to the appropriate mode of EAC separation (i.e., EAC mode, eddy mode or dipole mode). The assignment is done independently by each author, by eye, using the description of the modes by Ribbat et al. (2020); Roughan et al. (2022) as a guide (and shown in Figure 1). More information on mode assignment, A table summarizing the classification of each mission, and the offshore conditions, as well as composite sea level anomalies for glider days under each mode (Figure S1 in Supporting Information S1), prevailing wind conditions (Figure S2 in Supporting Information S1) and glider track coverage for each mode (Figure S3 in Supporting Information S1) can be found in Supporting Information. For the analysis below, we take the time-mean of each mission during the period when it is in our region of interest. This approach is taken for two reasons; First, each mission can be considered as an independent quasi-synoptic sample of the shelf circulation for a particular period (2–3 weeks), while individual profiles from the same mission are not independent from one another. Second, a mission-mean profile is taken at a length scale (order 100 km), which is resolved by the satellite altimetry, meaning we are considering the EAC separation mode and the shelf response at the same time and space scales.

When the mean $chla_{glider}$ for each mission is plotted, and split by season (Figure 8), the effect of separation mode on chlorophyll distribution is consistent with that observed in the individual case studies above. As could be expected, there is a large amount of variability between missions, due to differences in local winds, preceding conditions, interannual variability and other local impacts such as freshwater inputs. Due to the possibility of sensor-to-sensor variability, here we focus on the subsurface chlorophyll structure, rather than the absolute values. However, EAC mode gliders (Figure 8a) generally have the lowest $chla_{glider}$ and often have surface maxima. There appears to be little seasonality in both $chla_{glider}$ (Figure 8a) and density (Figure 8d). Eddy mode gliders show slightly higher $chla_{glider}$ values (Figure 8b), and exhibit several examples of shallow subsurface chlorophyll maxima, often more than 1 mg m^{-3} and centered at 20–30 m depth. There is a clear seasonal cycle in density, with missions in the warm months being more

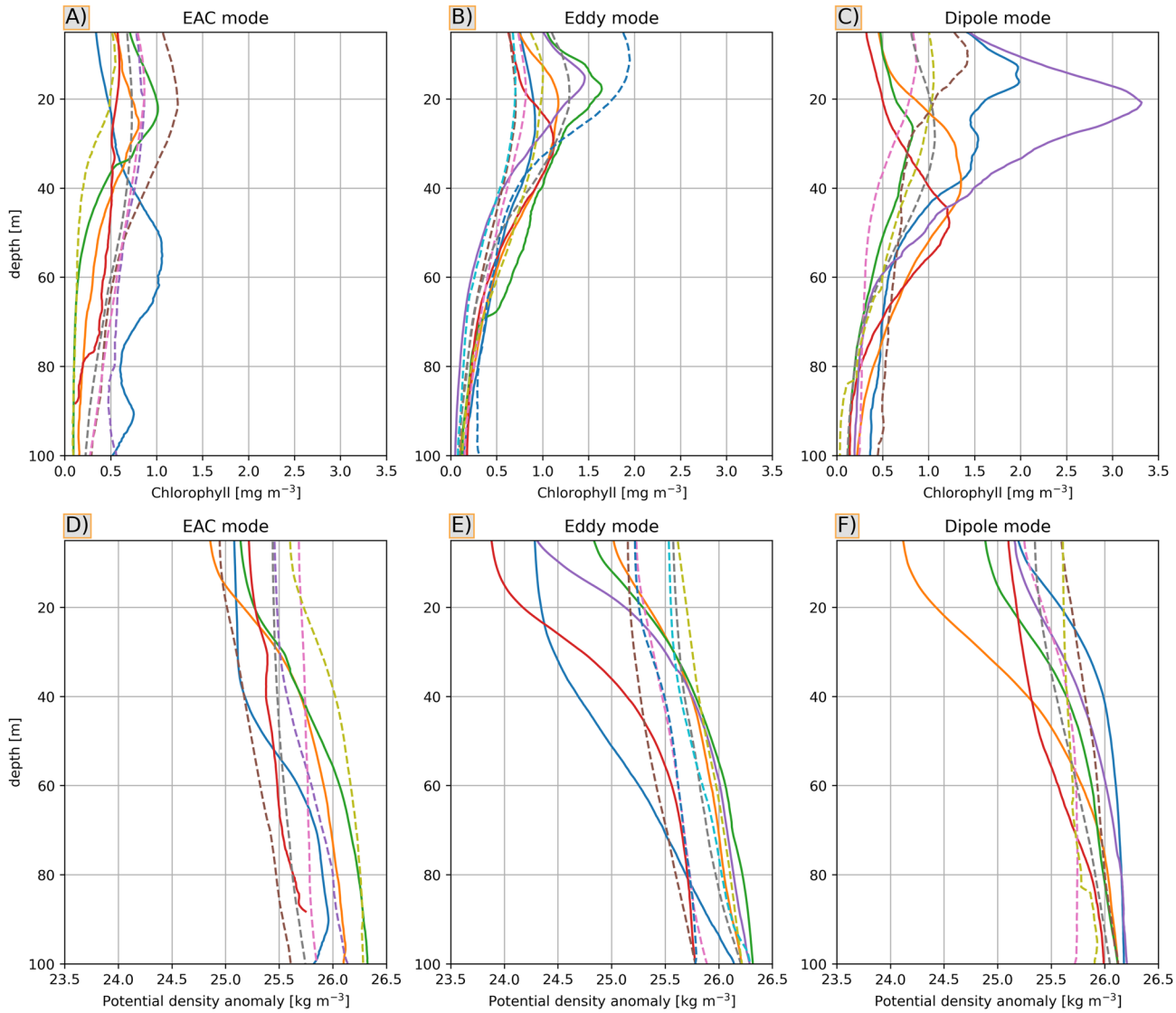

Figure 8. Time-mean Chlorophyll-a fluorescence (a–c) and potential density anomaly (d–f) profiles for the top 100 m of the water column taken over the period each glider is inshore of the 200 m isobath between 31.5°S and 34°S. The time-mean from each mission is grouped according to the mesoscale circulation mode at the time. Colors indicate the 29 different glider missions, with dashed lines showing missions taking place in cool months (May–Oct), and solid lines missions taking place in warm months (November–April).

stratified (Figure 8e). The dipole mode gliders (Figure 8c) show the largest values, but also the greatest range of different $chla_{glider}$ profiles. Subsurface chlorophyll maxima are common, especially in the warm months, and deeper than those observed in the eddy mode gliders, with several gliders sampling subsurface maxima below 30 m. A particular mission, in November 2020, had a time-mean chlorophyll maxima in excess of 3 mg m^{-3}. Further examination of the mesoscale conditions during this November 2020 mission shows that the shelf was impacted by consecutive eddy dipoles over this period (see Table S1 in Supporting Information S1). Density profiles during dipole mode missions (Figure 8f) show a similar pattern to those of the eddy mode, with stronger stratification in warm month missions.

The composite mean density (Figure 9a) and $chla_{glider}$ (Figure 9b) profiles of the 29 glider missions split by separation mode shows clear differences in stratification and chlorophyll distribution in the water column. As seen in the case studies, the shelf waters during the EAC mode are the least stratified and have the lowest $chla_{glider}$ values with surface maxima. The shelf waters during the eddy mode are more stratified and have a mean $chla_{glider}$ of 1 mg m^{-3} at 20 m. During the dipole separation mode, stratification is similar to, or marginally stronger than the eddy mode, particularly in the 30–80 m depth range. This is associated with higher $chla_{glider}$ values, and a defined subsurface chlorophyll maximum extending from 20 to 40 m deep.

When the effect of non-photochemical quenching (Falkowski & Kiefer, 1985) on the composite means of $chla_{glider}$ is compensated for by only using night-time profiles (following Schaeffer, Roughan, Jones, and White (2016), dashed lines in Figure 9b) the difference in vertical chlorophyll distribution between the three separation modes is highlighted. In general the quenching effect is not large on this scale. However, it reveals that during the EAC mode, chlorophyll is usually distributed evenly from the surface to the thermocline, while in the dipole mode, and to a lesser extent in the eddy mode, there are strong subsurface chlorophyll maxima which would not be detectable from the surface. An independent sample *t*-test reveals with 90% confidence ($p = 0.1$) that at depths between 15 and 80 m, mean night-time $chla_{glider}$ concentrations are greater during the dipole mode of separation when compared to the EAC mode of separation. The possibility of sensor-to-sensor variability could affect this result, but is thought to be small and not affect observed vertical structure (see Supporting Information for further discussion of glider calibration uncertainty). Differences in wind-driven coastal upwelling (e.g., if there were more upwelling favorable winds under the dipole mode) do not appear to account for the difference in chlorophyll concentrations between the EAC and dipole separation modes. In fact, the winds associated with the dipole mode are weakly downwelling in the mean and winds across all three separation modes do not appear to show a sustained upwelling or downwelling pattern (see Figure S2 in Supporting Information S1).

The subsurface chlorophyll maxima associated with the eddy and dipole modes of separation explain why the seasonality at depths greater than 10 m is opposite in phase to that seen from the surface in the satellite data (Figure 2d). At the surface, both the satellite and gliders show chlorophyll to be higher in the cooler (May-October) months. However, at depth the reverse is true due to the effect of the subsurface chlorophyll maxima common in the warmer months under the eddy and dipole modes of separation. An independent sample *t*-test reveals with 90% confidence ($p = 0.1$) that at depths between 15 and 80 m, mean night-time $chla_{glider}$ concentrations are greater during the warm months (November–April), compared to the cool months (May–October). Thus, the difference between warm and cool months stratification and subsurface chlorophyll on the shelf is in opposition to the seasonal cycle reported at the surface by (Everett et al., 2014) and is driven by the influence of the eddy and particularly the dipole mode of separation.

5. Discussion

Using three case studies, as well as composite data from 29 glider missions, we show that the subsurface distribution of chlorophyll on the continental shelf is strongly influenced by the mesoscale EAC and eddy circulation; particularly the mode in which the EAC jet separates from the coast and the eddy configuration. During the EAC mode of separation, the water column on the shelf is well-mixed, and the chlorophyll maximum tends to be mixed through the top 20–30 m. During the eddy mode of separation, composite mean subsurface $chla_{glider}$ values are 25% higher (Figure 9b), with a shallow subsurface chlorophyll maximum, and a more stratified water column. The dipole mode of separation has composite mean $chla_{glider}$ values twice that of the EAC mode (Figure 9b), with a defined subsurface chlorophyll maximum visible in the composite mean at depths of 20–40 m. The differences between modes are more marked in the warm months, when the stratification is stronger and the mesoscale circulation is more vigorous (Figure 2e). As the three separation modes of the EAC are mesoscale and derived from satellite altimetry data that explicitly do not resolve the shelf circulation, it appears that the offshore mesoscale circulation exerts a strong "top down" control on the distribution of chlorophyll on the shelf.

Here we discuss what drives the chlorophyll distribution between the three different modes of separation. It was previously established that upwelling due to the separation of the coherent EAC jet from the coast could be responsible for the maintenance of a persistent pool of nutrients at depth on the Hawkesbury Shelf (Roughan & Middleton, 2002; Schaeffer & Roughan, 2015). When we consider our three case studies, there is a potential for greater separation-driven upwelling during the eddy and dipole separation modes due to the more abrupt separation of the coherent EAC jet from the shelf (see Figures 4d and 4f). However, during the EAC mode, a current-driven uplift caused by the bottom stress of the strong EAC on the shallow edge of the continental slope, can explain the influx of nutrient rich upwelled waters (Roughan & Middleton, 2002; Schaeffer et al., 2014), although this process is inherently weaker as it is focused through the bottom boundary layer (Roughan & Middleton, 2002). Considering the relatively wide Hawkesbury Shelf, this process is also likely to be less efficient than along a narrow shelf, for example, further north at 30°S as per Schaeffer et al. (2013).

But upwelling alone does not account for the difference in subsurface chlorophyll values between the eddy and dipole modes. Previous studies on eddy dipoles in the EAC separation have shown that high levels of surface chlorophyll (>1 mg m^{-3}) are associated with the offshore interaction between the cyclonic and anticyclonic

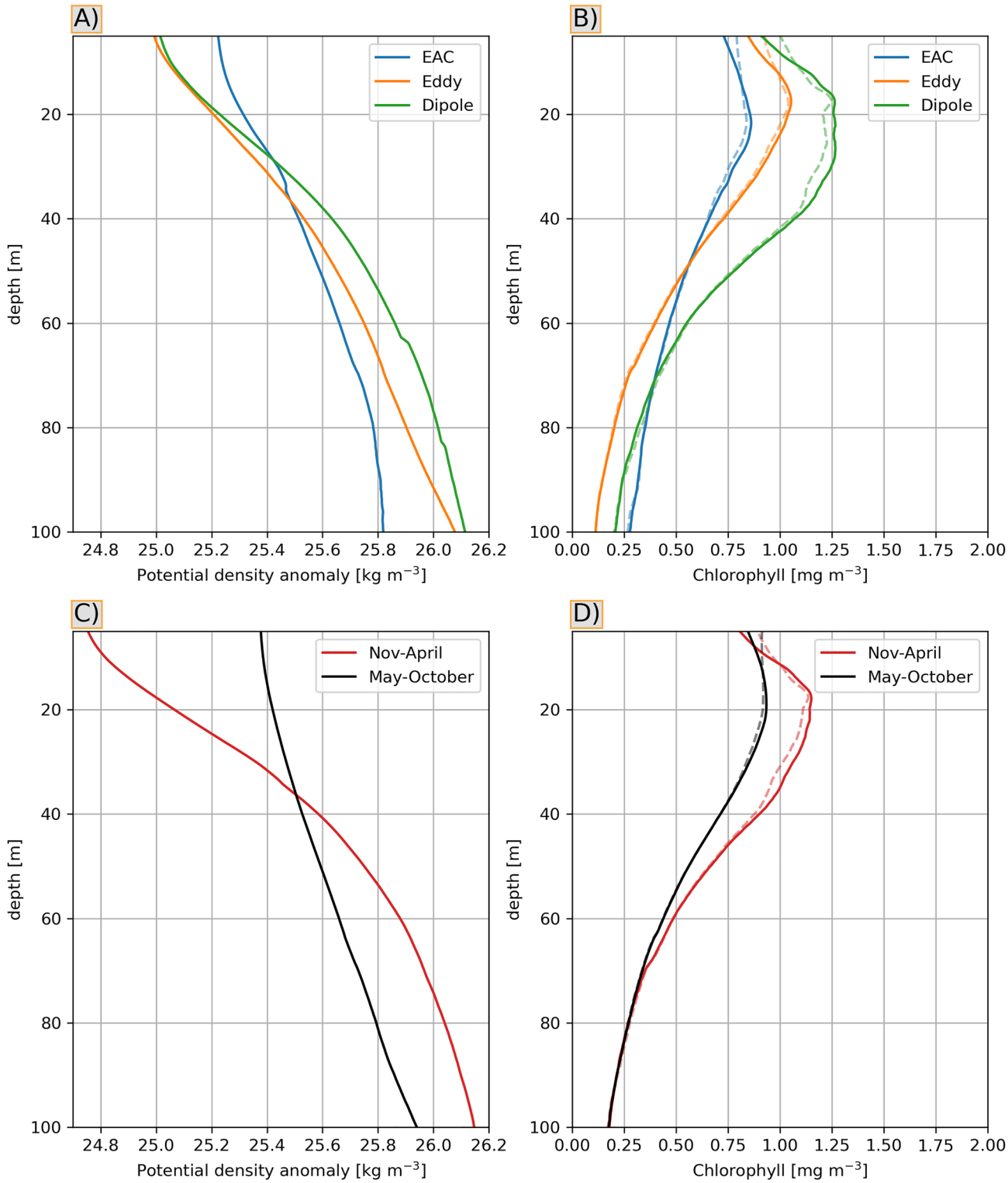

Figure 9. Composite mean profiles of (a) potential density anomaly and (b) $chla_{glider}$ for the EAC, Eddy and Dipole separation modes. (c) and (d) show the same analysis, but with profiles instead averaged by season. In (b) and (d), dashed lines show night time values only. Note that November–April represents the warm months and May–October the cooler months.

parts of the eddy dipole (Archer et al., 2020). This productive offshore water can then be advected shoreward and subducted under the surface water on the shelf (Malan et al., 2020). We hypothesize that this interaction between the offshore and shelf water due to the eddy dipole acts to connect the high chlorophyll, high nutrient water offshore with that on the continental shelf, creating a subsurface chlorophyll maximum which extends the full width of the shelf. An example of this offshore extent of chlorophyll is visible from the glider observations in Figure 5h. This is in agreement with Roughan and Middleton (2002) who used a nutrient climatology to show that upwelling through the Hawkesbury Shelf region was widespread through the watercolumn. However they did not consider the role of eddies in driving or maintaining the nutrient pool. The positioning of a subsurface chlorophyll maximum directly above the pycnocline (Figure 5i) on a stratified mid-latitude shelf has also been observed in other regions. Becherer et al. (2022), investigated the dynamics maintaining the subsurface chlorophyll maximum in the North Sea. For shelf stratification analogous to what we observe in the dipole mode, they found that stirring driven by tidal currents caused turbulence in the pycnocline, which entrained nutrients up into the subsurface chlorophyll maximum. While the effect of tidal currents on the Hawkesbury Shelf is small, the advection driven by the eddy dipole jet would provide a similar stirring effect, causing vertical current shear in the stratified shelf water which mixes nutrients upwards across the pycnocline to fuel the subsurface chlorophyll maximum.

The glider data set reveals a temporal shift in the timing of the surface and subsurface chlorophyll maxima. Surface chlorophyll values (from both satellite and glider observations) are highest in the cooler months (May to October), particularly September and October. Subsurface chlorophyll, on the other hand, is highest in the warmer months (November to April) and lowest in the cooler months (May to October, Figure 9d). However, the gliders (Figures 8a–8c) reveal that this subsurface seasonality can mostly be attributed to eddy and dipole separation mode conditions. This is likely due to the fact that the poleward flow in the EAC is stronger in summer at this latitude (Figure 2e), creating greater potential for separation-driven upwelling during the eddy and dipole separation modes. The high levels of subsurface chlorophyll associated with the dipole separation mode are not observable from satellite remote sensing, which is restricted to the first optical depth (Cornec et al., 2021; Morel et al., 1991), explaining the phase lag between surface chlorophyll, which is highest during the spring bloom (September-October, Figure 2d), and subsurface chlorophyll, which is highest in the warm months, at least 2 months later (Figure 9d). Thus, we find that the time-mean subsurface chlorophyll maximum reported by Schaeffer, Roughan, Austin, et al. (2016) is controlled primarily by the separation mode of the EAC and the associated cyclonic eddy configuration.

In terms of impact on air-sea exchange of carbon dioxide in this region, the dipole separation mode is particularly interesting. Mid-latitude continental shelves are generally sinks of atmospheric CO_2 (Bauer et al., 2013; Cai et al., 2006), and a limited modeling case study has shown this to hold true for the EAC (Macdonald et al., 2009). The strength of this sink is determined by two mechanisms, the biological and physical carbon pumps (Laruelle et al., 2018). Considering it simplistically, higher subsurface chlorophyll values point toward a stronger biological carbon pump during dipole separation modes. The key control on the physical carbon pump is whether CO_2 can be exchanged from the shelf to the deep ocean faster than it is exchanged from the atmosphere into the shelf waters (Laruelle et al., 2018). When the EAC is in dipole separation mode, cross-shelf exchange is increased, with export of water from the shelf due to more abrupt EAC separation, and import due to the dipole circulation. This is clear from our estimated cross-shelf transport in Figure 7c, and in agreement with accurate model-based cross-shelf transport calculations during eddy dipole events (Malan et al., 2022), which show large cross-shelf transport values (order 10 Sv). Thus, the dipole mode of EAC separation creates conditions under which we would expect the Hawkesbury Shelf to be a stronger carbon sink when compared to the other two separation modes. This shows the importance of resolving the full variability of the EAC separation when estimating carbon fluxes. For example, Macdonald et al. (2009) use two 21-day model simulations to investigate carbon fluxes and thus only capture a single mode of EAC separation (the EAC mode), possibly leading to underestimation as we have shown that this mode may have the least cross-shelf transport and weakest chlorophyll maxima.

6. Conclusions

The shelf waters inshore of western boundary currents are dynamically complex, sensitive to the impacts of climate change (Li et al., 2022a; Malan et al., 2021; Yang et al., 2020) and lie adjacent to coastlines which generally have large human populations. Furthermore, the subduction processes associated with the small-scale eddies and jets typical of western boundary current interactions with shelf waters have been associated with carbon export (Omand et al., 2015) in these hotspots of ocean carbon uptake (Nickford et al., 2022). Here, we used

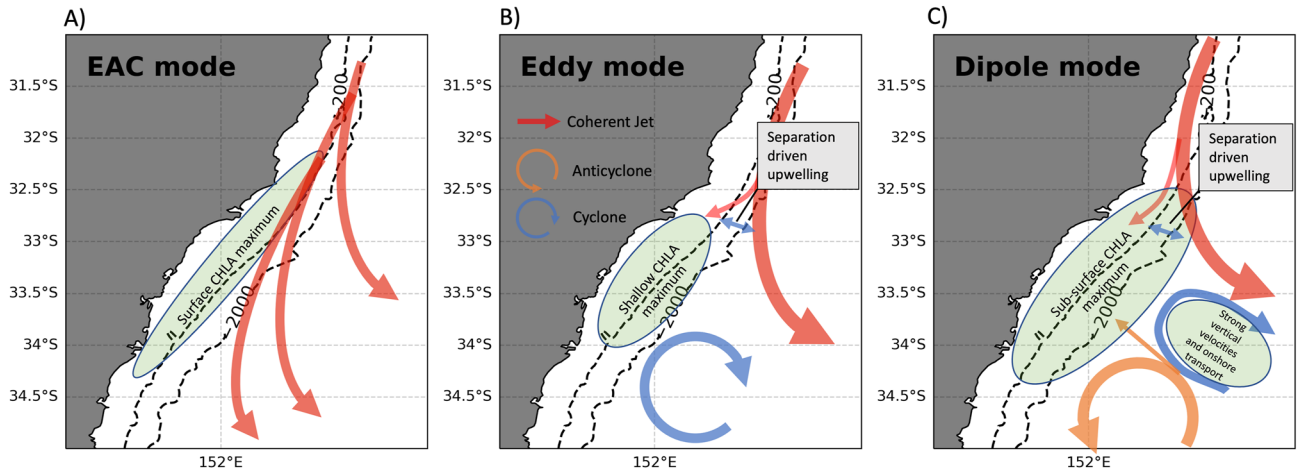

Figure 10. A schematic view of the three modes of chlorophyll distribution in the Hawkesbury Shelf during the warm months (November to April). Red arrows denote the coherent EAC jet, blue circles are cyclonic mesoscale eddies, orange circles are anticyclonic mesoscale eddies. The orange arrow shows the cross-shelf jet associated with the eddy dipole.

detailed observations from HF radar, 29 underwater glider missions, and satellite remote sensing to show that the mode of separation of the East Australian Current affects both the depth and strength of the chlorophyll maxima on the shelf and the stratification of the shelf water column. Underwater gliders reveal subsurface chlorophyll maxima associated with the eddy and dipole modes of EAC separation which have not been accounted for in previous studies using satellite data. The influence of the mode of EAC separation on the shelf persists in both time and space, and the influence of different modes of EAC separation appears to drive a seasonal cycle at depth, peaking in the warm months, which differs from that at the surface. Strong subsurface chlorophyll maxima on the shelf are especially common when eddy dipoles are present in the EAC separation, and link the productive coastal waters with offshore chlorophyll hotspots driven by the interaction of the counter-rotating mesoscale eddy dipoles.

We summarize our new paradigm in Figure 10 that gives a schematic view of how the three mesoscale modes of EAC separation drive chlorophyll distribution on the adjacent shelf. The schematic is based on the warm months, when differences between modes are clearest. When the EAC separation is most coherent ("EAC mode," Figure 10a) chlorophyll is mainly confined to the surface close to the coast. As the level of eddy variability increases, with the influence of a cyclonic eddy and earlier EAC separation, chlorophyll is deeper in the water column and tends to extend slightly further offshore due to greater separation-driven upwelling ("Eddy mode," Figure 10b). In the presence of an eddy dipole ("Dipole mode" Figure 10c) subsurface chlorophyll maxima are more common, and the productive coastal water links with offshore productivity associated with the cyclonic side of the dipole. These results are supported by the view of Roughan et al. (2022) who identified the importance of the cyclonic eddy in controlling the mesoscale interaction of the WBC with the shelf circulation and thus cross-shelf transport. The cross-shelf jet driven by the eddy dipole (Figure 10c) acts as the mechanism by which the offshore and coastal chlorophyll is linked, resulting in a large area of high subsurface chlorophyll values as well as cross-shelf exchange. Our results show the importance of offshore mesoscale context in shaping shelf chlorophyll distributions and highlight that the use of satellite data, or a simple time-mean approach, may result in an underestimation of the productivity of this shelf region and its importance to both regional ecosystems and the biological carbon pump.

Data Availability Statement

All datasets analysed for this study can be found on the Australian Ocean Data Network https://portal.aodn.org.au. Altimetry (IMOS, 2022a), http://thredds.aodn.org.au/thredds/catalog/IMOS/OceanCurrent/GSLA/DM01/catalog.html. SST (IMOS, 2022d), http://thredds.aodn.org.au/thredds/catalog/IMOS/SRS/SST/ghrsst/L3S-1d/ngt/catalog.html. Ocean colour (IMOS, 2022e), http://thredds.aodn.org.au/thredds/catalog/IMOS/SRS/OC/gridded/aqua/catalog.html. HF radar (IMOS, 2022b), http://thredds.aodn.org.au/thredds/catalog/IMOS/ACORN/gridded_1h-avg-current-map_QC/NEWC/catalog.html. Glider (IMOS, 2022c), http://thredds.aodn.org.au/thredds/catalog/IMOS/ANFOG/slocum_glider/catalog.html. The Supporting Information also uses wind data from ERA5 (Hersbach et al., 2018), https://www.ecmwf.int/en/forecasts/datasets/reanalysis-datasets/era5.

Acknowledgments
The authors would like to acknowledge the work of the IMOS glider and radar field teams over the last decade in making this data set possible. Data were sourced from Australia's Integrated Marine Observing System (IMOS)—IMOS is enabled by the National Collaborative Research Infrastructure Strategy (NCRIS). Open access publishing facilitated by University of New South Wales, as part of the Wiley - University of New South Wales agreement via the Council of Australian University Librarians.

References

Archer, M. R., Schaeffer, A., Keating, S., Roughan, M., Holmes, R., & Siegelman, L. (2020). Observations of submesoscale variability and frontal subduction within the mesoscale eddy field of the Tasman Sea. *Journal of Physical Oceanography*, *50*(5), 1509–1529. https://doi.org/10.1175/JPO-D-19-0131.1

Bauer, J. E., Cai, W. J., Raymond, P. A., Bianchi, T. S., Hopkinson, C. S., & Regnier, P. A. (2013). The changing carbon cycle of the coastal ocean. *Nature*, *504*(7478), 61–70. https://doi.org/10.1038/nature12857

Becherer, J., Burchard, H., Carpenter, J. R., Graewe, U., & Merckelbach, L. M. (2022). The role of turbulence in fueling the subsurface chlorophyll maximum in tidally dominated shelf seas. *Journal of Geophysical Research: Oceans*, *127*(8), e2022JC018561. https://doi.org/10.1029/2022JC018561

Bull, C. Y., Kiss, A. E., Jourdain, N. C., England, M. H., & van Sebille, E. (2017). Wind forced variability in eddy formation, eddy shedding, and the separation of the East Australian current. *Journal of Geophysical Research: Oceans*, *122*(12), 9980–9998. https://doi.org/10.1002/2017JC013311

Bureau of Meteorology. (2022). Summary statistics Nelson Bay (Nelson Head). Retrieved from http://www.bom.gov.au/climate/averages/tables/cw_061054.shtmlhttp://www.bom.gov.au/climate/averages/tables/cw_061054.shtml

Cai, W. J., Dai, M., & Wang, Y. (2006). Air-sea exchange of carbon dioxide in ocean margins: A province-based synthesis. *Geophysical Research Letters*, *33*(12), 2–5. https://doi.org/10.1029/2006GL026219

Carr, M. E., Friedrichs, M. A., Schmeltz, M., Noguchi Aita, M., Antoine, D., Arrigo, K. R., et al. (2006). A comparison of global estimates of marine primary production from ocean color. *Deep-Sea Research Part II Topical Studies in Oceanography*, *53*(5–7), 741–770. https://doi.org/10.1016/j.dsr2.2006.01.028

Carr, M. E., & Kearns, E. J. (2003). Production regimes in four eastern boundary current systems. *Deep-Sea Research Part II: Topical Studies in Oceanography*, *50*(22–26), 3199–3221. https://doi.org/10.1016/j.dsr2.2003.07.015

Cetina-Heredia, P., Roughan, M., Liggins, G., Coleman, M. A., & Jeffs, A. (2019b). Mesoscale circulation determines broad spatio-temporal settlement patterns of lobster. *PLoS One*, *14*(2), 1–20. https://doi.org/10.1371/journal.pone.0211722

Cetina-Heredia, P., Roughan, M., Sebille, E., Keating, S., & Brassington, G. B. (2019a). Retention and leakage of water by mesoscale eddies in the East Australian current system. *Journal of Geophysical Research: Oceans*, *124*(4), 2485–2500. https://doi.org/10.1029/2018JC014482

Cetina-Heredia, P., Roughan, M., van Sebille, E., & Coleman, M. A. (2014). Long-term trends in the East Australian Current separation latitude and eddy driven transport. *Journal of Geophysical Research: Oceans*, *119*(7), 4351–4366. https://doi.org/10.1002/2014JC010071

Cornec, M., Claustre, H., Mignot, A., Guidi, L., Lacour, L., Poteau, A., et al. (2021). Deep chlorophyll maxima in the global ocean: Occurrences, drivers and characteristics. *Global Biogeochemical Cycles*, *35*(4). https://doi.org/10.1029/2020GB006759

Cosoli, S. (2020). Implementation of the listen-before-talk mode for seasonde high-frequency ocean radars. *Journal of Marine Science and Engineering*, *8*(1), 1–14. https://doi.org/10.3390/JMSE8010057

Cosoli, S., & Grcic, B. (2019). *Quality control procedures for IMOS ocean radar manual version 2.1*. (Technical Report, November). Integrated Marine Observing System. Retrieved from http://content.aodn.org.au/Documents/IMOS/Facilities/ocean_radar/QC_procedures_for_IMOS_Ocean_Radar_manual_v2.1.pdf

Cullen, J. J. (2015). Subsurface chlorophyll maximum layers: Enduring enigma or mystery solved? *Annual Review of Marine Science*, *7*(September 2014), 207–239. https://doi.org/10.1146/annurev-marine-010213-135111

Deng, X., Griffin, D. A., Ridgway, K., Church, J. A., Featherstone, W. E., White, N. J., & Cahill, M. (2011). Satellite altimetry for geodetic, oceanographic, and climate studies in the Australian region. In *Coastal altimetry* (pp. 473–508). Springer Berlin Heidelberg. https://doi.org/10.1007/978-3-642-12796-0(_)18

de Vos, S. J., Cosoli, S., & Munroe, J. (2020). The traveling wave loop antenna: A terminated wire loop aerial for directional high-frequency ocean radar transmission. *Remote Sensing*, *12*(17), 1–30. https://doi.org/10.3390/rs12172800

Everett, J. D., Baird, M. E., Roughan, M., Suthers, I. M., & Doblin, M. A. (2014). Relative impact of seasonal and oceanographic drivers on surface chlorophyll a along a Western Boundary Current. *Progress in Oceanography*, *120*, 340–351. https://doi.org/10.1016/j.pocean.2013.10.016

Falkowski, P., & Kiefer, D. A. (1985). Chlorophyll a fluorescence in phytoplankton: Relationship to photosynthesis and biomass. *Journal of Plankton Research*, *7*(5), 715–731. https://doi.org/10.1093/plankt/7.5.715

Fassbender, A. J., Palter, J. B., Long, M. C., Ito, T., Bishop, S. P., & Cronin, M. F. (2018). Ocean carbon hot spots: A joint US Clivar and OCB workshop report. (Technical Report).

Gregor, L., Ryan-Keogh, T. J., Nicholson, S. A., du Plessis, M., Giddy, I., & Swart, S. (2019). GliderTools: A Python Toolbox for processing underwater glider data. *Frontiers in Marine Science*, *6*(December), 1–13. https://doi.org/10.3389/fmars.2019.00738

Griffin, C., Beggs, H., & Majewski, L. (2017). GHRSST compliant AVHRR SST products over the Australian region. (Technical Report). Retrieved from http://imos.org.au/fileadmin/user_upload/shared/SRS/SST/GHRSST-DOC-basic-v1.0r1.pdf

Hersbach, H., Bell, B., Berrisford, P., Biavati, G., Horányi, A., Muñoz Sabater, N. J. J., et al. (2018). ERA5 hourly data on single levels from 1959 to present [Dataset]. Copernicus Climate Change Service (C3S) Climate Data Store (CDS). https://doi.org/10.24381/cds.adbb2d47

IMOS. (2022a). Gridded (adjusted) sea level anomaly (GSLA), gridded sea level (GSL) and surface geostrophic velocity (UCUR,VCUR) over the Australian domain between 1993-01-01T00:00 and 2021-03-13T00:00 [Dataset]. Retrieved from https://catalogue-imos.aodn.org.au/geonetwork/srv/eng/catalog.search#/metadata/c68b6e1b-98a6-415e-8563-f526e1db1bd5

IMOS. (2022b). IMOS-ACORN-Newcastle HF ocean radar site (New South Wales, Australia)-delayed mode sea water velocity between 2017-11-30 and 2021-09-16 [Dataset]. Retrieved from https://catalogue-imos.aodn.org.au/geonetwork/srv/eng/catalog.search#/metadata/6dca1f8a-8337-4551-ac4b-a2d35ec6f333

IMOS. (2022c). IMOS-Australian National Facility for Ocean Gliders (ANFOG)-delayed mode glider deployments, for the east coast region 31.5–34 S [Dataset]. Retrieved from https://portal.aodn.org.au/search?uuid=37662a66-ec3a-4ece-9db0-31930c181725

IMOS. (2022d). IMOS L3S Day and Night gridded multiple-sensor multiple-swath Australian region HRPT AVHRR foundation SST, 1992-03-21T09:20:00Z, 2022-04-17T09:20:00Z [Dataset]. Retrieved from https://catalogue-imos.aodn.org.au/geonetwork/srv/eng/catalog.search#/metadata/a136eee7-a990-4c06-a4f6-915657a2464e

IMOS. (2022e). IMOS-SRS-MODIS-01day-Chlorophyll-aconcentration(OC3model)between2002-07-04T05:30and2022-03-31T05:30[Dataset]. Retrieved from https://catalogue-imos.aodn.org.au/geonetwork/srv/eng/catalog.search#/metadata/d7a14921-8f3f-4522-9a54-e7d1df969c8a

Jacox, M. G., Edwards, C. A., Kahru, M., Rudnick, D. L., & Kudela, R. M. (2015). The potential for improving remote primary productivity estimates through subsurface chlorophyll and irradiance measurement. *Deep-Sea Research Part II Topical Studies in Oceanography*, *112*, 107–116. https://doi.org/10.1016/j.dsr2.2013.12.008

Laruelle, G. G., Cai, W. J., Hu, X., Gruber, N., Mackenzie, F. T., & Regnier, P. (2018). Continental shelves as a variable but increasing global sink for atmospheric carbon dioxide. *Nature Communications*, *9*(1), 454. https://doi.org/10.1038/s41467-017-02738-z

Levy, M., Bopp, L., Karleskind, P., Resplandy, L., Ethe, C., & Pinsard, F. (2013). Physical pathways for carbon transfers between the surface mixed layer and the ocean interior. *Global Biogeochemical Cycles*, *27*(4), 1001–1012. https://doi.org/10.1002/gbc.20092

Li, J., Roughan, M., & Kerry, C. (2021). Dynamics of interannual eddy kinetic energy modulations in a Western Boundary Current. *Geophysical Research Letters*, *48*(19), e2021GL094115. https://doi.org/10.1029/2021gl094115

Li, J., Roughan, M., & Kerry, C. (2022a). Drivers of ocean warming in the Western boundary currents of the Southern Hemisphere. *Nature Climate Change*, *12*(10), 901–909. https://doi.org/10.1038/s41558-022-01473-8

Li, J., Roughan, M., & Kerry, C. G. (2022b). Variability and drivers of ocean temperature extremes in a warming Western boundary current. *Journal of Climate*, *35*(3), 1097–1111. https://doi.org/10.1175/jcli-d-21-0622.1

Li, J., Roughan, M., Kerry, C., & Rao, S. (2022). Impact of mesoscale circulation on the structure of river Plumes during large rainfall events inshore of the East Australian current. *Frontiers in Marine Science*, *9*(815348). https://doi.org/10.3389/fmars.2022.815348

Lucas, A. J., Dupont, C. L., Tai, V., Largier, J. L., Palenik, B., & Franks, P. J. (2011). The green ribbon: Multiscale physical control of phytoplankton productivity and community structure over a narrow continental shelf. *Limnology & Oceanography*, *56*(2), 611–626. https://doi.org/10.4319/lo.2011.56.2.0611

Macdonald, H. S., Baird, M. E., & Middleton, J. H. (2009). Effect of wind on continental shelf carbon fluxes off southeast Australia: A numerical model. *Journal of Geophysical Research*, *114*(C5), C05016. https://doi.org/10.1029/2008JC004946

Malan, N., Archer, M., Roughan, M., Cetina-heredia, P., Hemming, M., Rocha, C., et al. (2020). Eddy-driven cross-shelf transport in the East Australian current separation zone. *Journal of Geophysical Research: Oceans*, *125*(2), 1–15. https://doi.org/10.1029/2019JC015613

Malan, N., Roughan, M., & Kerry, C. (2021). The rate of coastal temperature rise adjacent to a warming Western boundary current is nonuniform with latitude. *Geophysical Research Letters*, *48*(3), 1–10. https://doi.org/10.1029/2020GL090751

Malan, N., Roughan, M., Stanley, G. J., Holmes, R., & Li, J. (2022). Quantifying cross-shelf transport in the East Australian current system: A budget-based approach. *Journal of Physical Oceanography*, *52*(10), 2555–2572. https://doi.org/10.1175/JPO-D-21-0193.1

Morel, F. M. M., Hudson, R. J. M., & Price, N. M. (1991). Of productivity by trace metals in the sea. *Limnology*, *36*(8), 1742–1755. https://doi.org/10.4319/lo.1991.36.8.1742

Mullaney, T. J., & Suthers, I. M. (2013). Entrainment and retention of the coastal larval fish assemblage by a short-lived, submesoscale, frontal eddy of the East Australian Current. *Limnology & Oceanography*, *58*(5), 1546–1556. https://doi.org/10.4319/lo.2013.58.5.1546

Nickford, S., Palter, J. B., Donohue, K., Fassbender, A. J., Gray, A. R., Long, J., et al. (2022). Autonomous wintertime observations of air-sea exchange in the gulf stream reveal a perfect storm for ocean CO_2 uptake. *Geophysical Research Letters*, *49*(5). https://doi.org/10.1029/2021GL096805

Oke, P. R., & Middleton, J. (2001). Nutrient enrichment off Port Stephens: The role of the East Australian current. *Continental Shelf Research*, *21*(6–7), 587–606. https://doi.org/10.1016/s0278-4343(00)00127-8

Oliver, H., Zhang, W. G., Smith, W. O., Alatalo, P., Chappell, P. D., Hirzel, A. J., et al. (2021). Diatom hotspots driven by Western boundary current instability. *Geophysical Research Letters*, *48*(11), 1–10. https://doi.org/10.1029/2020GL091943

Omand, M. M., D'Asaro, E. A., Lee, C. M., Perry, M. J., Briggs, N., Cetinić, I., & Mahadevan, A. (2015). Eddy-driven subduction exports particulate organic carbon from the spring bloom. *Science*, *348*(6231), 222–225. https://doi.org/10.1126/science.1260062

Pauly, D., & Christensen, V. (1995). Primary production required to sustain global fisheries. *Nature*, *374*(6519), 255–257. https://doi.org/10.1038/374255a0

Pilo, G. S., Oke, P. R., Coleman, R., Rykova, T., & Ridgway, K. (2018). Patterns of vertical velocity induced by eddy distortion in an ocean model. *Journal of Geophysical Research: Oceans*, *123*(3), 2274–2292. https://doi.org/10.1002/2017JC013298

Renault, L., Deutsch, C., McWilliams, J. C., Frenzel, H., Liang, J.-H., & Colas, F. (2016). Partial decoupling of primary productivity from upwelling in the California Current system. *Nature Geoscience*, *9*(7), 505–508. https://doi.org/10.1038/ngeo2722

Ribbat, N., Roughan, M., Powell, B., Rao, S., & Kerry, C. G. (2020). Transport variability over the Hawkesbury shelf (31.5-34.5°S) driven by the East Australian current. *PLoS One*, *15*(11 November), 1–27. https://doi.org/10.1371/journal.pone.0241622

Roughan, M., Cetina-Heredia, P., Ribbat, N., & Suthers, I. M. (2022). Shelf transport pathways adjacent to the East Australian current reveal sources of productivity for coastal Reefs. *Frontiers in Marine Science*, *8*, 1970. https://doi.org/10.3389/fmars.2021.789687

Roughan, M., Keating, S. R., Schaeffer, A., Cetina-Heredia, P., Rocha, C., Griffin, D., et al. (2017). A tale of two eddies: The biophysical characteristics of two contrasting cyclonic eddies in the East Australia Current System. *Journal of Geophysical Research: Oceans*, *122*(3), 2494–2518. https://doi.org/10.1002/2016JC012241

Roughan, M., & Middleton, J. H. (2002). A comparison of observed upwelling mechanisms off the East Coast of Australia. *Continental Shelf Research*, *22*(17), 2551–2572. https://doi.org/10.1016/S0278-4343(02)00101-2

Roughan, M., Schaeffer, A., & Suthers, I. M. (2015). Sustained Ocean observing along the coast of southeastern Australia: NSW-IMOS 2007-2014. In *Coastal ocean observing systems* (pp. 76–98). Elsevier Inc. https://doi.org/10.1016/B978-0-12-802022-7.00006-7

Schaeffer, A., & Roughan, M. (2015). Influence of a Western boundary current on shelf dynamics and upwelling from repeat glider deployments. *Geophysical Research Letters*, *42*(1), 121–128. https://doi.org/10.1002/2014GL062260

Schaeffer, A., Roughan, M., Austin, T., Everett, J. D., Griffin, D., Hollings, B., et al. (2016a). Mean hydrography on the continental shelf from 26 repeat glider deployments along Southeastern Australia. *Scientific Data*, *3*(1), 160070. https://doi.org/10.1038/sdata.2016.70

Schaeffer, A., Roughan, M., Jones, E. M., & White, D. (2016b). Physical and biogeochemical spatial scales of variability in the East Australian Current separation from shelf glider measurements. *Biogeosciences*, *13*(6), 1967–1975. https://doi.org/10.5194/bg-13-1967-2016

Schaeffer, A., Roughan, M., & Morris, B. D. (2013). Cross-shelf dynamics in a Western boundary current regime: Implications for upwelling. *Journal of Physical Oceanography*, *43*(5), 1042–1059. https://doi.org/10.1175/JPO-D-12-0177.1

Schaeffer, A., Roughan, M., & Wood, J. E. (2014). Observed bottom boundary layer transport and uplift on the continental shelf adjacent to a Western boundary current. *Journal of Geophysical Research: Oceans*, *119*(8), 4922–4939. https://doi.org/10.1002/2013JC009735

Schollaert, S. E., Rossby, T., & Yoder, J. A. (2004). Gulf Stream cross-frontal exchange: Possible mechanisms to explain interannual variations in phytoplankton chlorophyll in the slope sea during the SeaWiFS years. *Deep Sea Research Part II: Topical Studies in Oceanography*, *51*(1–3), 173–188. https://doi.org/10.1016/J.DSR2.2003.07.017

Schroeder, T., Lovell, J., King, E., Clementson, L., & Scott, R. (2017). *Ocean colour validation report 2016–2017. Report to the integrated marine observing system (IMOS)* (Vol. 33). CSIRO Oceans and Atmosphere.

Testor, P., DeYoung, B., Rudnick, D. L., Glenn, S., Hayes, D., Lee, C., et al. (2019). OceanGliders: A component of the integrated GOOS. *Frontiers in Marine Science*, *6*, 422. https://doi.org/10.3389/FMARS.2019.00422

Todd, R. E., Chavez, F. P., Clayton, S., Cravatte, S., Goes, M., Graco, M., et al. (2019). Global perspectives on observing ocean boundary current systems. *Frontiers in Marine Science*, *6*, 423. https://doi.org/10.3389/fmars.2019.00423

Woo, M. (2019). Ocean Gliders delayed mode QA/QC best practice manual Version 2.0. (Technical Report).

Yang, H., Lohmann, G., Krebs-Kanzow, U., Ionita, M., Shi, X., Sidorenko, D., et al. (2020). Poleward shift of the major ocean gyres detected in a warming climate. *Geophysical Research Letters*, *47*(5). https://doi.org/10.1029/2019GL085868